Computational Materials Science 197 (2021) 110650

Contents lists available at ScienceDirect

Computational Materials Science

journal homepage: www.elsevier.com/locate/commatsci

3D percolation modeling for predicting the thermal conductivity of graphene-polymer composites

Asghar Aryanfar [a,b,*], Sajed Medlej [a], Ali Tarhini [a], S. Reza Damadi [c], Ali R. Tehrani B. [d], William A. Goddard III [e]

[a] American University of Beirut, Riad El-Solh 1107, Lebanon
[b] Bahçeşehir University, 4 Çırağan Cad, Beşiktaş, Istanbul 34353, Turkey
[c] University of Tabriz, 29 Bahman Blvd, Tabriz, Iran
[d] Aalto University, Chemical Engineering, Espoo 02150, Finland
[e] California Institute of Technology, 1200 California Blvd, Pasadena, CA 91125, United States

ARTICLE INFO

Keywords:
Composite polymer
Percolation
Elliptic fillers
Thermal conductivity

ABSTRACT

Graphene-based polymer composites exhibit a microstructure formed by aggregates within a matrix with enhanced thermal conductivity. We develop a percolation-based computational method, based on the multiple runnings of the shortest path iteratively for ellipsoidal particles to predict the thermal conductivity of such composites across stochastically-developed channels. We analyze the role of the shape and the aspect ratio of the flakes and we predict the onset of percolation based on the density and particle dimensions. Consequently, we complement and verify the conductivity trends via our experiments by inclusion of graphene aggregates and fabrication of graphene-polymer composites. The analytical development and the numerical simulations are successfully verified with the experiments, where the prediction could explain the role of larger set of particle geometry and density. Such percolation-based quantification is very useful for the effective utilization and optimization of the equivalent shape of the graphene flakes and their distribution across the composite during the preparation process and application.

1. Introduction

Polymer composites with augmented thermal conductivity values are promising materials with potential applications in industries such as electronics and renewable energy systems [1,2]. Polymers have very low in-plane thermal conductivity with less than 0.2 $W.m^{-1}.K^{-1}$ for polyvinylidene fluoride-co-hexafluoropropylene (PVDF-HFP) [3], therefore the insertion of highly conductive graphene fillers of up to 5000 $W.m^{-1}.K^{-1}$ could improve the conductivity dramatically [4–6], allowing them to be utilized in new applications [2,4,7,8]. Additionally their piezo-resistive behavior on strain sensitivity enables them for application in structural health monitoring [2,9].

Graphene's high thermal conductivity is related to the small phonon scattering within defect free mono-layer particles [10]. But such particle inclusions possess large surface areas that create significant interfacial contact with polymers and amplifies surface scattering [2]. Thus, the determining factors for the homogenized thermal conductivity depend on the filler and matrix material, as well as their interface. These factors can be classified as: (1) The characteristics of graphene used (percentage of defects, average particle size, aspect ratio), (2) The dispersion of graphene flakes within the composite, (3) The loading of Graphene (*volume*% or *weight*%), and (4) The interfacial contact resistance between the polymer matrix and the Graphene filler [2,11]. The efficient computation of these parameters have potential for quantifying the thermal conductivity of Graphene-based composites [12,13] where the verification with experimental data could attain a reliable way to study the effect of Graphene *wt*% and particle size on the thermal properties of graphene-based composites.

Percolation theory and fractal dynamics have been at the heart of modeling the behavior and transport of properties in composite media [14–16] from the hydraulic conductivity in fractal soil [17] to the conductance of spheroidal biological suspensions [18]. The fractal models assume that the medium resembles a truncated domain [19] where their properties such as the thermal conductivity κ obeys a power law above the percolation threshold as follows:

* Corresponding author.
E-mail address: aryanfar@caltech.edu (A. Aryanfar).

https://doi.org/10.1016/j.commatsci.2021.110650
Received 5 April 2021; Received in revised form 3 June 2021; Accepted 6 June 2021
Available online 20 June 2021

$$\kappa \sim (p - p_c)^t$$

where p is the volume fraction of the filler phase, p_c is the volume fraction at the percolation threshold, and t is the conductivity exponent which depends on the geometry and distribution of the conducting filler [20]. However, this exponent is dynamically calculated signifying the non-universality of the percolation behavior in conductive-insulating media [21], especially when approaching the percolation threshold from above as the medium becomes highly anisotropic due to the high tortuosity of conducting pathways [22]. Hence, the effective conduction is highly altered by the level of connectedness of the conductive phase which can be achieved by carbon nanotubes at very low filling percentages [23], as well as the thickness of the conductive pathways [24]. This understanding aided in enhancing the performance of mixtures, notably polymer graphene composites, based on the structural properties as well as the production methods and post-production routines [25].

Researchers also relied on approximations in General Effective Media (GEM) [26–28] to predict the physical properties, while others refuted old classical models with emulsions [29]. The ultimate conductivity of binary medium depends on the conductivity of both media, the critical volume fraction, and the power exponent which either represents the fractal dimension, conductor–insulator transition point, or the effective demagnetization coefficient of the grain structure [30,31]. On the other hand the Finite Volume Methods (FVM) and Monte Carlo simulations have been used to calculate the electrical conductivity of PVDF/Graphene and other conducting-insulating composites [32,33] verifying the power law. These results also showed the conductivity depends on the spatial distribution of fillers within the matrix as they transition from stochastic to Gaussian. In addition, the percolation limits for conductance decreases with filler aspect ratio. Other models of computing the conductivity in continuum percolation media use random-walk algorithms over well defined boundaries inside the mixtures [34].

On the other hand, numerical simulations are a powerful tool for predicting the physical properties of graphene-based composites [35–37], which could help optimize the preparation process and improve desirable physical properties. The finite element method has been utilized for heat transfer of graphene foam (GF) within polydimethylsiloxane (PDMS) polymeric composite by Zhang et al. [36] and 3*D* models are used for the thermal behavior of graphene nano-platelets (GNPs) in epoxy composites. Of the investigated physical properties are the radius to thickness ratio, the interfacial thermal conductivity, and the agglomeration degree of the graphene nano-platelets within the composite [37]. Other approaches include molecular dynamics simulations for applications in wearable devices, under uniaxial tensile strain, and vertical stress [38]. Similar studies determine the effect of porosity on the thermal conductivity of a single-layer of Graphene [39]. Non-equilibrium molecular dynamics (NEMD) simulations also studied the thermal properties of the nano-porous Graphene (NPG) sheets used as thermo-electric materials, which aids in tuning the thermal conductivity in NPG sheets by altering graphene porosity [40]. Nevertheless, a more versatile and faster method based on particle shape is needed to quantitatively estimate the conductive channels, which would highly enrich the understanding of heat propagation within these composites.

In this paper, we have developed a new percolation-based 3D method to compute the thermal conductivity of polymeric composites, whilst the connection pattern of the graphene flakes within the polymeric solutions is complex due to the number of pathways available within the composite. The link between the geometry of the graphene flakes and it's surface area is studied and correlated to the thermal conductivity. The method has been implemented and assessed with our experimental data and therefore can be used for predicting conductivity of graphene-contained polymer in the larger space of parameters for particle size and shape as well as the density of the aggregates.

2. Methodology

2.1. Modeling

The graphene flakes are assumed to have ellipsoid shapes with variant aspect ratio. Here we develop a framework for predicting the effective thermal conductivity based on continuum elliptic percolation via stochastic simulations of specific realizations related to the dimensions of ellipses. Fig. 1 schematically characterizes the different patterns of such random media. Ellipsoidal zones denoted by "0" represent lone islands of congregated particles that are not connected to any percolated pathway. The set denoted by "1" represents partially percolated pathways, and they vary in reach and width depending on the dispersion. The last set denoted by "2" consists of complete percolation pathways between the opposite edges of domain. This set is the most effective for conduction identifying such routes is the focus of our study.

The numerical model consists of three major phases preceded by the initialization of the ellipses as shown in Fig. 2. The particles are stochastically generated with coordinates (x_i, y_i, z_i) with respective stochastic yaw, pitch, and roll orientations $(\alpha_i,\ \beta_i,\ \gamma_i)$, where $\{x_i, y_i, z_i\} \in [0, 1]$ and $\{\alpha_i, \beta_i, \gamma_i\} \in [0, \pi]$. Although the orientation angle vary over all quadrants, the limitation of these angles in the first two quadrants will ensure the symmetry of the percolation properties in the orthogonal directions of the plane. In addition, the particles dimensions are specified as $\{a, b, c\}$ being the semi-major and two semi-minor axes of the ellipsoids, and N is the multiplicity of the particles. The geometric dimensions of the ellipses are generated proportionally to the boundary length of the normalized domain such that the particles in-plane dimensions match that of the graphene flakes provided in the experimental section. Hence we define the aspect ratio as $r_{2D} := \frac{b}{a}$ and $r_{3D} := \frac{c}{a}$ varied between $r \in \{0.01, 0.2\}$ to identify the parameters that properly represent the graphene-polymer medium. The equation of an individual ellipsoid with semi-major and two semi-minor axes (a, b, c) centered at the position (x_0, y_0, z_0) and rotated by the angles (α, β, γ) is given by:

$$(\mathbf{X} - \mathbf{X}_0)^T \mathbf{R}^T \mathbf{A} \mathbf{R} (\mathbf{X} - \mathbf{X}_0) = 1$$

where $X$is the position vector defined as:

$$\mathbf{X} = \begin{bmatrix} x \\ y \\ z \end{bmatrix}$$

and $\mathbf{X}_0$ is the center position as:

$$\mathbf{X}_0 = \begin{bmatrix} x_0 \\ y_0 \\ z_0 \end{bmatrix}$$

$\mathbf{R}$ is the general rotation matrix comprised of the multiplication of the 3 basic rotation matrices about the principal axes, and is given as:

$$\begin{aligned} \mathbf{R} &= R_x(\alpha) R_y(\beta) R_z(\gamma) \\ &= \begin{bmatrix} 1 & 0 & 0 \\ 0 & cos\alpha & -sin\alpha \\ 0 & sin\alpha & cos\alpha \end{bmatrix} \begin{bmatrix} cos\beta & 0 & -sin\beta \\ 0 & 1 & 0 \\ sin\beta & 0 & cos\beta \end{bmatrix} \begin{bmatrix} cos\gamma & -sin\gamma & 0 \\ sin\gamma & cos\gamma & 0 \\ 0 & 0 & 1 \end{bmatrix} \end{aligned}$$

and $\mathbf{A}$ is a scaling matrix defined as:

$$\mathbf{A} = \begin{bmatrix} \frac{1}{a^2} & 0 & 0 \\ 0 & \frac{1}{b^2} & 0 \\ 0 & 0 & \frac{1}{c^2} \end{bmatrix}$$

Aided by the simplicity of matrix multiplication, a set of N ellipsoids is generated at each realization, where each ellipsoid E_i has its own

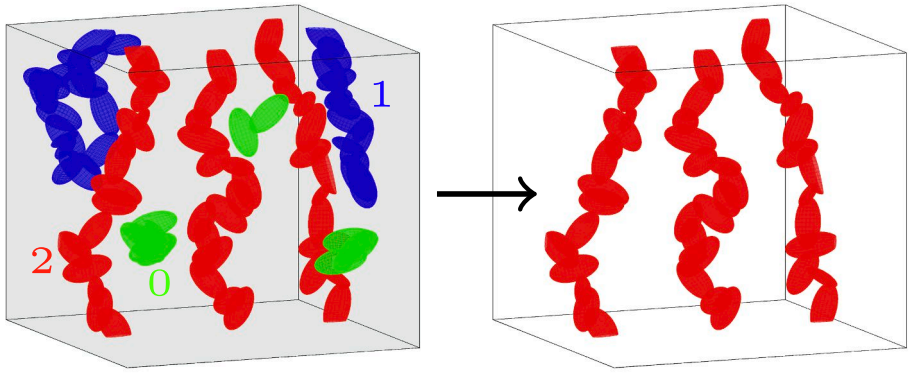

Fig. 1. Schematics of percolation representing full, partial and separated particle chains [41].

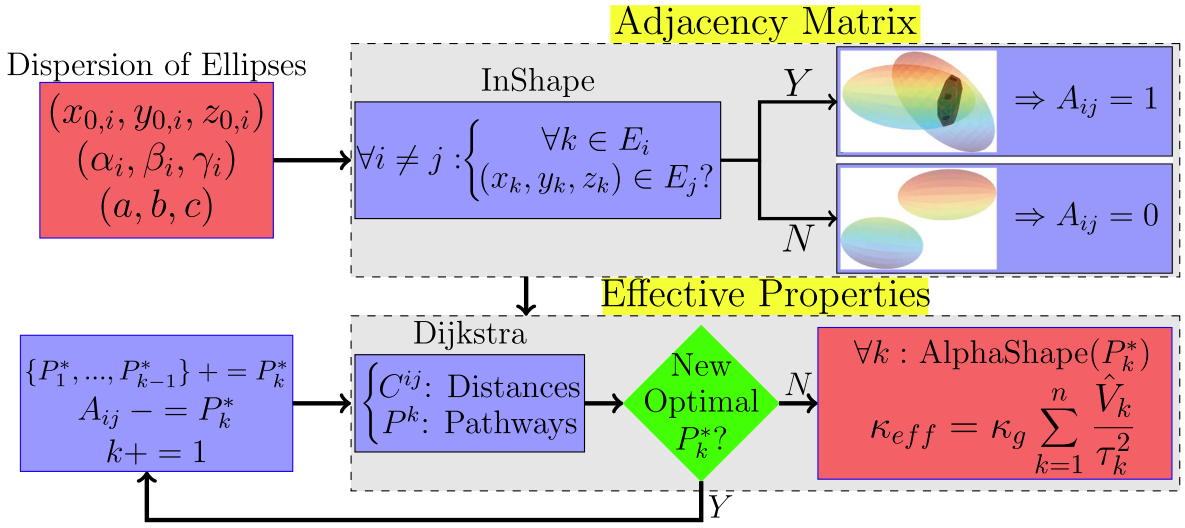

Fig. 2. Pseudo-flowchart for extracting the homogenized conductivity.

stochastic position and orientation. The ellipsoid surface points $\mathbf{X}_i$ are generated using MATLAB's built-in function "*ellipsoid*" and applying the rotation matrix $\mathbf{R}_i$ for each ellipsoid individually.

The connection of ellipsoids is then identified by the adjacency matrix A_{ij} of size $(N \times N)$ in the domain of each realization for computing percolation through the entire medium, which is then utilized to investigate the presence of percolation pathways. Having possessed the surface points of all ellipsoids E_i, we use another MATLAB built-in function "*alphaShape*" to generate convex closed objects from the sets of surface points. In this manner, we were able to deal with each ellipse as one object instead of a group of surface points. This also allowed us to take advantage of supporting functions in MATLAB for *alphaShape*, precisely the function "*inShape*" which identifies if a selected point belongs to an *alphaShape*. Hence, for each ellipsoid E_i, we checked if the surface points of other ellipsoid $E_{j\neq i}$ lie in it and set the corresponding A_{ij} to 0 or 1 depending on the boolean result. However,

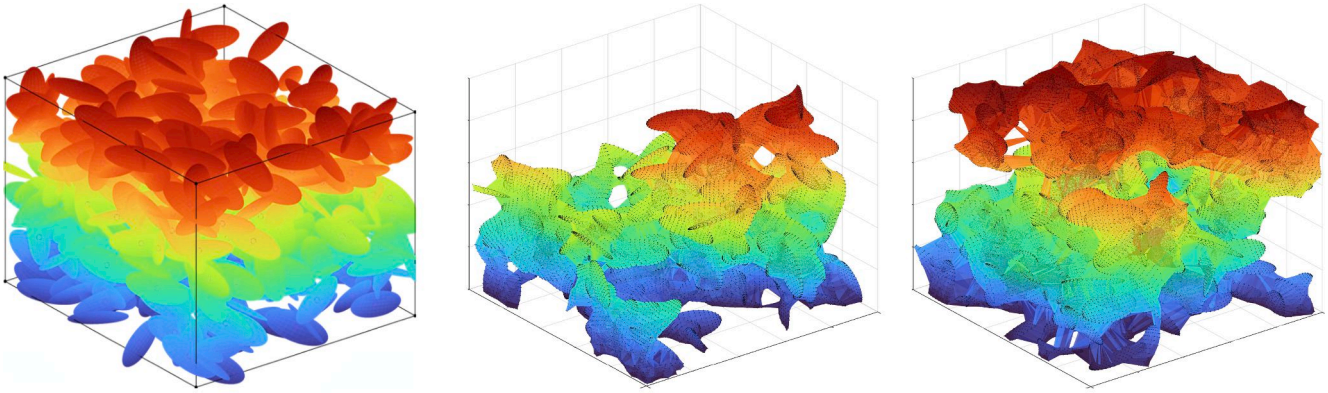

(a) Sample ellipsoids in domain (b) Partial percolation cluster (c) Full percolation cluster

Fig. 3. Simulation realizations showing dispersed particles in the domain and the percolation cluster in case of availability or unavailability of full percolation pathways.

only close enough ellipsoids are checked for intersection to reduce the computational cost of the simulations (i.e. only for $|\mathbf{X}_j - \mathbf{X}_i| \leq 2{\cdot}max\{a,b,c\}$). (see Fig. 3).

Subsequently, continuum percolation is performed at each iteration depending on the available connected ellipsoids from the edges of the medium, and shortest connecting pathways are selected. Consequently, it is added to the list of percolation pathways, and new unique and optimal pathways are re-scanned for iteratively until none are found. For optimal path detection, the Dijkstra's algorithm is utilized [42], which is not only used for elliptical percolation [43,44], but also proved beneficial in, and not limited to, path-planning [45–47], chemical particle distribution [48], combustion kinetics [49], and anatomical therapeutic drugs detection [50].

The Dijkstra algorithm depends on contacting ellipsoids and assigns costs for paths as the normal distance between the centers of the ellipses in comprising the path. For this purpose, the adjacency matrix A_{ij} computed above is coupled with the positions of the particles (x_i, y_i, z_i) to compute the normal distances and generate the costs matrix C_{ij}. These costs are represented by the blue segments in the Fig. 4a, and show the background graph of connections. The algorithm starts from a set of ellipsoids at one edge of the domain and finds locally minimum cost connections to reach the final destination at the opposite edge. The search for the starting and ending particles is limited to those within a distance of $max\{a,b,c\}$ from any of the boundary faces. Whenever a new shorter path is found through a different, but not necessarily unique set of connected ellipsoids, the previous longer path is replaced by the new optimized path. Fig. 4b shows for a randomly generated set of ellipsoids the only unique and most optimum percolation paths.

A significant intermediate parameter for non-percolating cases is the cluster size of partial connection from only one face ($\widehat{V}_{part}$) which is normalized by the domain volume and computed using the Burn algorithm [51]. The burning propagates with forward percolation as it starts from one corner of the domain, and moves sequentially through the connected particles via 1^{st}-order neighbors until no further progress is made. Additional computed parameters include the normalized volume of pathways $\widehat{V}_i$ and their respective tortuosities τ_i. The computation of overlapped volumes can be performed via "alphaShape" MATLAB toolkit. The merged non-uniform shape is illustrated by comparing the intersections of red particles in Fig. 4a and the joined color-coded pathways in 4b.

The individual tortuousity τ_i is calculated as:

$$\tau_i = \frac{l_i}{d_i} \tag{1}$$

where l_i and d_i are the total length and shortest distance between the path edges. As well, the effective homogenized conductivity κ_{eff} can be calculated given the individual tortuosities of partial and full percolation pathways of graphene chains, τ_p and τ_f respectively, according to the following formulation [52–54]:

$$\begin{aligned}\kappa_{eff} &= p\kappa_{eff,f} + (1-p)\kappa_{eff,p} \\ &= p\kappa_g \sum \frac{\widehat{V}_{i,f}}{\tau_{i,f}^2} + (1-p)\left(\frac{1}{\kappa_g \sum\left(\frac{rabh_i}{\tau_{i,p}}\right)} + \frac{1}{\kappa_{pm}(1-h_i)}\right)^{-1}\end{aligned} \tag{2}$$

where $\kappa_{eff,f}$ and $\kappa_{eff,p}$ is the effective conductivity of the full and partial percolation pathways. As well, κ_g and κ_{pm} are the thermal conductivity of the graphene and the polymer respectively, p is the percolation probability, and h is the height of the pathway farthest away from the percolation starting edge, and $\widehat{V}_i$ is the normalized volume of an optimal percolation pathway summed for all unique ones at each realization of the simulation. Needless to mention that the conductivity of the graphene particles could be variant due to smaller scale properties (i.e. defects, inhomogeneities, etc.) which could be explored as a next step and herein we assume homogenous matter, in the scale considered. As well the estimation of the porosity $\widehat{V}_{tot}$ is computed via the following equation [55]:

$$\widehat{V}_{tot} = 1 - e^{-N\frac{V_e}{V_d}} \tag{3}$$

where V_d is the volume of the simulated domain, and $V_e = \pi abc = \pi r a^2 b$ is the volume of a single ellipse. $\widehat{V}_{tot}$ is thus the total filling volume of the particles in the domain representing the graphene phase, calculated based on the excluded volume principle. The dimension of the experimental particle dimensions (next section) could vary in the different directions, Hence, the $3D$ ellipsoid particles modeled here are the idealized imitation from the $2D$ experimental images of graphene flakes.

2.2. Experimental

A set of composite samples where prepared by mixing 98.5% pure

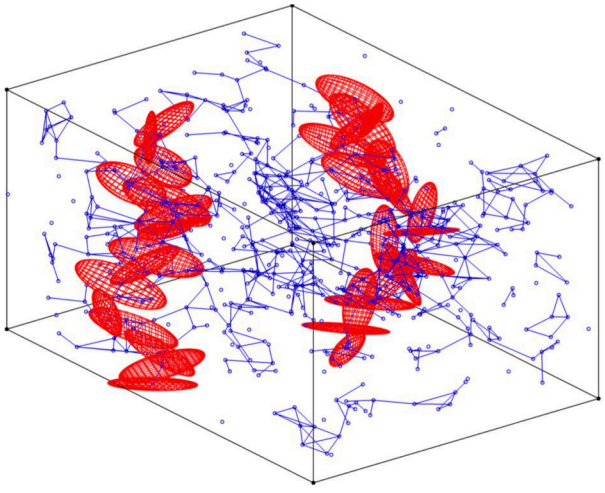

(a) Partial percolation pathways overlaid via the fully connecting ellipsoidal clusters.

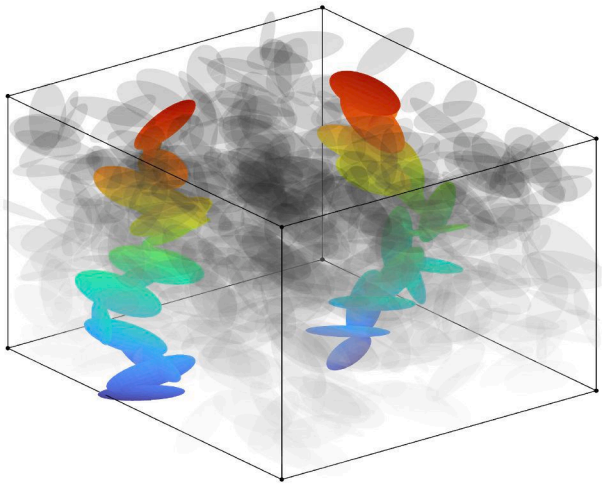

(b) Indexed particles based on their proximity to the percolation boundary.

Fig. 4. Stochastic percolation of elliptic particles with $r = 0.1$ and $N = 300$.

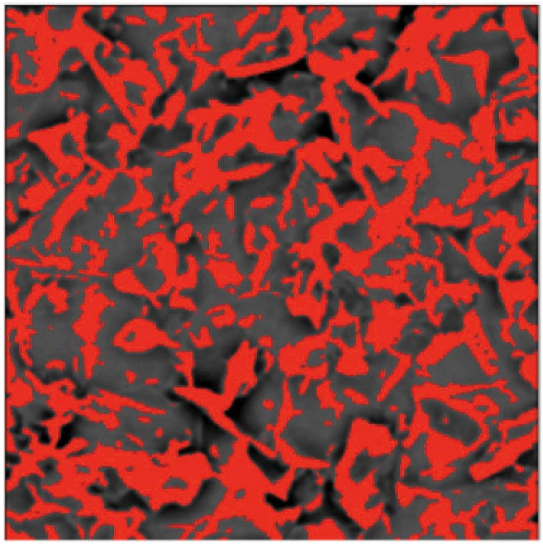

(a) Binarized image for $\hat{w}_g \approx 0.25$

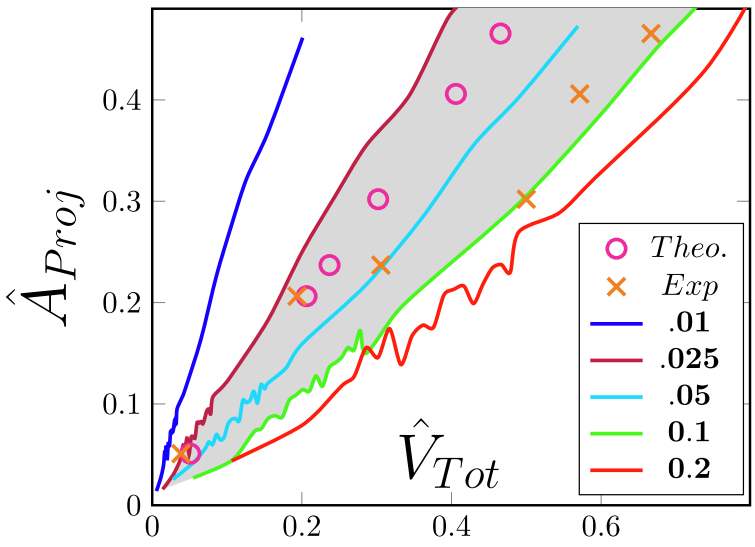

(b) Projected area for the utilized methods.

Fig. 5. Sample binarized SEM image of graphene-polymer specimen and its extracted projected surface area plotted against model predictions for multiple particle aspect ratios.

graphene flakes with PVDF-HEP polymer at graphene weight percentages $\hat{w}_g$ varying between 0.1% to 50% (see Table 1) in a silicon mold of dimensions $(3.5 \times 3.5 \times 3.5)\ cm^3$. The synthesis process is comprised of four steps: mixing, molding, evaporating the polymer solvent, and heating, which are described in detail in [56]. Moreover, the graphene flakes are assumed to have an ellipsoidal shape with dimensions $\sim (7 \times 3.5 \times 0.001)\ \mu m^3$ as provided by the supplier and verified by Scanning Electron Microscope images [56].

An example of the investigated SEM images is shown in Fig. 5a where graphene flakes are highlighted in red and polymer in gray. The SEM images of the experimental samples were used to extract the graphene area ratio $\hat{A}_{Exp}$ with an error of $< 6\%$ using ImageJ software which utilizes Otsu's thresholding method [57], where values below the threshold represent the composite polymer and graphene flakes otherwise. Additionally, the 3*D* mass ratio was correlated with the in-plane 2D properties of SEM images using dimensional analysis as follows:

$$A \propto V^{\frac{2}{3}} \propto M^{\frac{2}{3}} \tag{4}$$

Equation 4 in fact provides a bird-view relationship between 2*D* experimental images and 3*D* simulations, therefore the effect of anisotropic physical properties and defects is omitted as a negligible value. Therefore having the weight (i.e. mass) ratios in the Table 1 we calculate the respective theoretical area ratio $\hat{A}_{Theo.}$. The experimental and theoretical graphene surface areas are plotted against the projected area $\hat{A}_{proj.}$ of surface ellipsoids for and array of $r_{3D} \in [0.01, 0.2]$ using our numerical simulations in Fig. 5b. Both $\hat{A}_{Exp}$ and $\hat{A}_{Theo}$ lie between projected areas of ellipsoids with $r_{3D} = 0.025$ and $r_{3D} = 0.1$ indicating that the equivalent aspect ratios of the flakes lies in such range.

The value for the heat capacity c_p of each sample was measured using a differential scanning calorimeter Q2000 TA Instruments. The in-plane thermal diffusivity of each sample was measured using the laser flash diffusivity analyzer LFA 467 HyperFlash from Netzsch. A special holder was inserted inside two circular metallic masks where the lower mask had a central hole with a diameter $d_0 = 5\ mm$ allowing the laser beam to heat a circular region of the polymeric composite. Furthermore, the upper mask had two concentric circles of diameters $d_1 = 8\ mm$ and $d_2 = 10\ mm$, exposing the other side of the sample surface to an IR detector which measures the temperature rise in the sample. Then, the in-plane thermal conductivity was calculated in correlation with the cross-plane thermal diffusivity, laser pulse energy, the thickness of the film, pulse duration, and the sample holder's openings diameter. All measurements were calculated on samples with a diameter of 15 *mm* at Temperature $\sim 23\ ^\circ C$. The thermal diffusivity values were the average of 6 –8 consecutive measurements and thermal conductivity κ was calculated using the following equation:

$$\kappa = \alpha \rho_C c_p \tag{5}$$

where α is the thermal diffusivity, c_p is the heat capacity, and ρ is the density of each composite film. The thermal conductivity values for the selected graphene weight content are reported in Table 1.

Table 1
In-plane surface area fractions and thermal conductivity values for graphene-polymer composites with various graphene normalized weights $\hat{w}_g$.

$\hat{w}_g$ (*wt*)	$\hat{A}_{Theo.}$ (%)	$\hat{A}_{Exp.}$ (%)	$\kappa_{Exp.}$ $(W/m.K)$
0	0	0	0.22
0.01	5	5	3.24
0.06	15	21	7.95
0.1	21	24	15.99
0.2	34	30	24.53
0.25	40	41	36.33
0.33	48	47	38.06
0.5	63	62	57.21

3. Results & discussions

The percolation of the graphene clusters leading to the ultimate thermal conductivity can be highly influenced by the particles geometry and their respective aspect ratio [58–61]. The trend of the percolation pathways tortuosity in Fig. 6a shows asymptotic decrease towards its lower bound of $\tau = 1$. Therefore the high multiplicity of graphene particles offer shorter i.e. more straight pathways for percolation. The percolation threshold is the smallest for the lowest aspect ratio since the connection of these particles is dominated by their major axis which has a favorable reach inside the domain. On the contrary, the high aspect ratio particles ($r \to 1$) tend to accumulate more and with higher feasibility of overlapping albeit in directions that are unfavorable for completing full percolation pathways. Note that the saturation of the

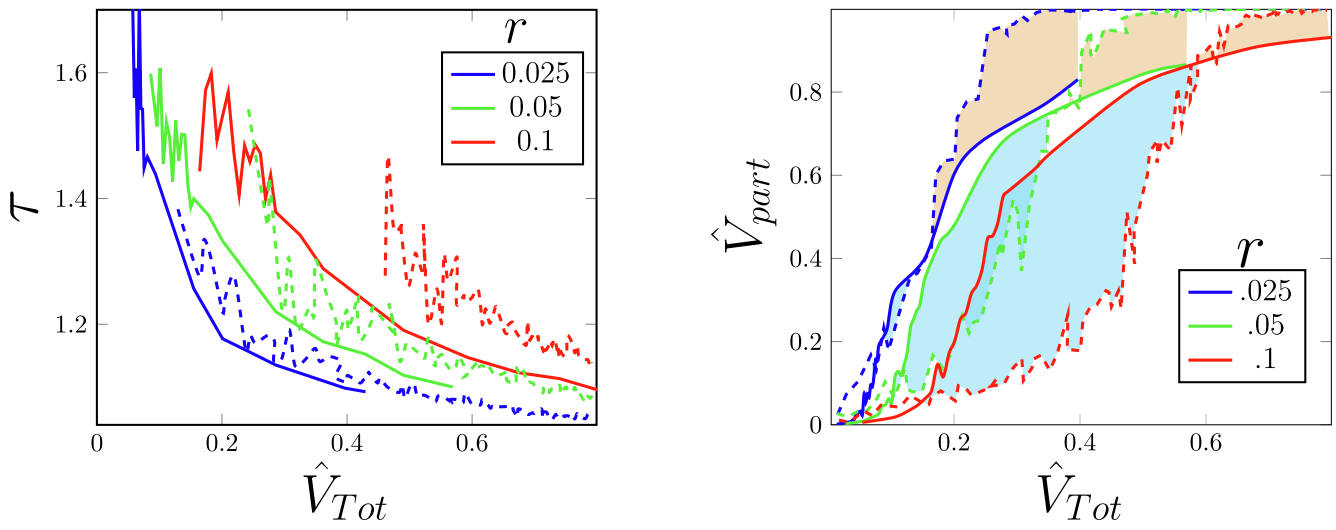

(a) Tortuosity. (b) Partial percolation volume.

Fig. 6. Normalized percolation parameters (solid: 3D, dashed: 2D).

total volume correlates non-linearly with the particle density in the domain via Eq. (3) [62,63,61]. Thus more graphene particles saturation provides higher conductivity.

As well in Fig. 6b the saturation in the partial percolation pathways volume $\hat{V}_{part}$ shows direct correlation with the original porosity $\hat{V}_{tot}$ of the ellipsoid aggregates in the domain. The early development of the volume of partial percolation clusters for particles with low aspect ratios is attributed to their low percolation threshold, but this development is less rapid compared to higher aspect ratio particles. As for 2*D* domains, the saturation behavior of partial percolation cluster density shows higher effectiveness than that of its 3*D* counterpart through a narrow transition window from island clusters to fully percolated pathways, denoted by "0" and "2" respectively in Fig. 1. Moreover, 2*D* particles demonstrated better capability of covering the domain for lower number densities because typically filling the medium in 3*D* needs more effort relative to 2*D*. The underlying reason is the in-out plane movement allowed by the additional propagation direction for percolation. However such mechanism is only useful at lower porosity where the connections are rare and the extra dimension offers more chances for the propagation of percolation, which is highlighted by the light blue region in Fig. 6b where 3*D* partial volumes stand higher. As the total filling volume increases and the saturation of the domain removes the connectivity issue after full percolation is achieved, the 2*D* filling fraction exceeds the 3*D* values. Such transition is highlighted in the Fig. 6b where it indicates a regime of original porosity where 3*D* movements is useful for connectivity albeit not so useful for filling the 3*D* domain after a certain saturation level.

Fig. 7a shows the experimental effective area derived from processing SEM images similar to the Fig. 5 and the simulated effective percolation pathway volumes for various aspect ratios ($\hat{V}_{eff} = \sum \hat{V}_i$) via flowchart 2. The experimental results presented against the plotted model computations correlates with the experiments for the chosen aspect ratios, although the similarity deteriorates for high aspect ratio ellipsoids at low original porosity. The aspect ratio of the graphene-

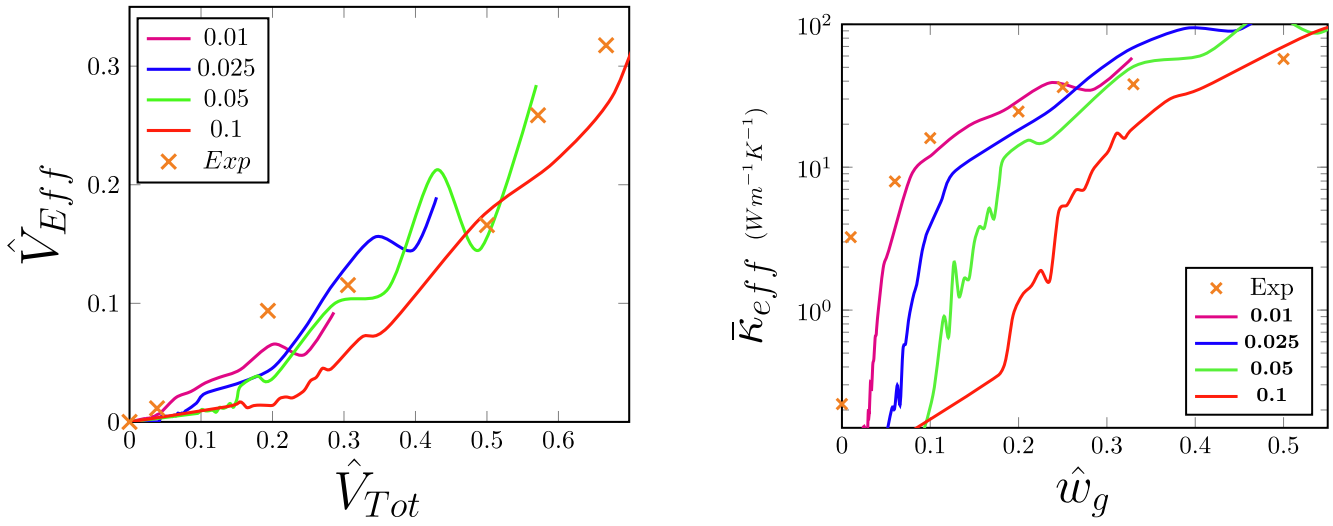

(a) Normalized volumes of the effective percolation pathways. (b) Thermal conductivity.

Fig. 7. Thermal conductivity of graphene-polymer composite versus the graphene filling weight ratio $\hat{w}_g$. cross: experimental values, solid curves: ellipsoidal simulations with multiple aspect ratios.

particles in the model resembles the strip-like agglomeration witnessed in Fig. 5. This behavior can be attributed to the fabrication process where graphene flakes aggregate to form thin interfaces adjacent to polyhedral polymer particles [64,65]. Additionally, The size and aspect ratio of graphene particles may change during the preparation of the composites due to high speed mechanical mixing of the graphene dispersion. As a result, the effective flake size of the graphene flakes may be different than the experimental measurements of individual flakes.

Therefore, we proceeded with calculating the total conductivity of the medium according to Eq. (2) for the set of aspect ratios of $r = \{0.01, 0.025, 0.05, 0.1\}$ for the proper applicability of continuum percolation theory to the experimental samples. It is worth mentioning that performing the simulations in 3*D* and the experiments have a subtle source of deviation. The simulations allow the ellipsoid particles to merge owing to their random positioning and orientation, contrary to the flakes in the experiments where there is no overlap of graphene flakes, which correlates with the 2*D* planar simulations of higher aspect ratio.

Without further analysis it is immediately apparent that the composite effective conductivity κ_{eff} falls in between the higher ($5000\ W.m^{-1}.K^{-1}$) and the lower ($0.2\ W.m^{-1}.K^{-1}$) conductivity values (Fig. 1). In fact:

$$\kappa_{pm} \leqslant \kappa_{eff} \leqslant \kappa_g$$

Fig. 7b shows the effective thermal conductivity of the graphene-polymer composite as a function of the original porosity of particles, where the experimental results (orange cross) are compared against the elliptic simulation values (solid curves). This figure shows the degree of compatibility between the model results and the experimental data relative to the particles aspect ratio, and it is apparent that as the aspect ratio decreases the model prediction improves on accuracy as seen for $r_{3D} = 0.01$. The significant influence of the aspect ratio is inferred from its ability to reduce the percolation threshold of the medium whilst filling a smaller volume of the domain, resulting in improved thermal conductivity for smaller graphene weight content [66–68]. Another observation is that particles of one aspect ratio are not accurate enough to solely explain the experimental results, and this is due to the fractal nature of the dispersed phase of graphene where the complex shapes could be approximated with multiple lower scale overlapping ellipsoids. The SEM images in Fig. 5 show that the larger particles of coagulated graphene are connected to smaller pigments that vary in aspect ratio and increase the fractal dimension of percolation pathways.

4. Conclusions

In this paper, we developed a new 3*D* numerical percolation model based on ellipsoidal particles for quantifying the effective thermal conductivity of Graphene-PVDF polymer film composites. The presented method is verified via developing a separate experimental measurement of thermal conductivity where we utilized two distinct methods of image processing and dimensional analysis for the experimental samples. We additionally analyzed the role of partial inclusion of graphene on the conductivity depending on the particle aspect ratio. The significant correlation between the model and experimental results provide insights to estimate the closest equivalent shape of graphene particles responsible for the effective conducting pathways. Additionally, the method can be used for predicting the homogenized physical properties to broader stochastically filler-matrix composites. Future works include the role of the variation in the particles shape and their multiplicity as well as the sensitivity analysis in the neighborhood of the percolation threshold.

CRediT authorship contribution statement

Asghar Aryanfar: Conceptualization, Validation, Formal analysis, Investigation, Writing - original draft, Writing - review & editing, Visualization, Funding acquisition. **Sajed Medlej:** Methodology, Data curation, Writing - review & editing. **S. Reza Damadi:** Data curation, Software, Writing - review & editing. **Ali R. Tehrani B.:** Supervision, Project administration. **William A. Goddard III:** Supervision, Project administration.

Declaration of Competing Interest

The authors declare that they have no known competing financial interests or personal relationships that could have appeared to influence the work reported in this paper.

Acknowledgement

The authors would like to thank and recognize the support from Masri Institute at American University of Beirut, Award#103919 and the PhD support from the Maroun Samaan Faculty of Engineering and Architecture for the student Sajed Medlej.

Appendix A. Supplementary data

Supplementary data associated with this article can be found, in the online version, at https://doi.org/10.1016/j.commatsci.2021.110650.

References

[1] Le Lv, Wen Dai, Aijun Li, Cheng-Te Lin, Graphene-based thermal interface materials: an application-oriented perspective on architecture design, Polymers 10 (11) (2018) 1201.
[2] An Li, Cong Zhang, Yang-Fei Zhang, Thermal conductivity of graphene-polymer composites: Mechanisms, properties, and applications, Polymers 9 (9) (2017) 437.
[3] A.A. Tarhini, A.R. Tehrani-Bagha, Graphene-based polymer composite films with enhanced mechanical properties and ultra-high in-plane thermal conductivity, Composites Science and Technology 184 (2019), 107797.
[4] Alexander A. Balandin, In-plane and cross-plane thermal conductivity of graphene: applications in thermal interface materials, in: Carbon Nanotubes, Graphene, and Associated Devices IV, 8101, International Society for Optics and Photonics, 2011, p. 810107.
[5] Yapeng Chen, Jingyao Gao, Qingwei Yan, Xiao Hou, Shengcheng Shu, Mingliang Wu, Nan Jiang, Xinming Li, Jian-Bin Xu, Cheng-Te Lin, et al. Advances in graphene-based polymer composites with high thermal conductivity. Veruscript Functional Nanomaterials, 2, 2018.
[6] Zhi-Ling Hou, Wei-Li Song, Ping Wang, Mohammed J Meziani, Chang Yi Kong, Ankoma Anderson, Halidan Maimaiti, Gregory E. LeCroy, Haijun Qian, Ya-Ping Sun, Flexible graphene–graphene composites of superior thermal and electrical transport properties. ACS Applied Materials & Interfaces 6(17) (2014) 15026–15032.
[7] Gunho Jo, Minhyeok Choe, Sangchul Lee, Woojin Park, Yung Ho Kahng, Takhee Lee, The application of graphene as electrodes in electrical and optical devices. Nanotechnology, 23(11) (2012) 112001.
[8] Alexander A Balandin, Suchismita Ghosh, Wenzhong Bao, Irene Calizo, Desalegne Teweldebrhan, Feng Miao, Chun Ning Lau, Superior thermal conductivity of single-layer graphene, Nano Letters 8(3) (2008) 902–907.
[9] Byeong-Cheol Kang, Ban-Suk Park, Tae-Jun Ha, Highly sensitive wearable glucose sensor systems based on functionalized single-wall carbon nanotubes with glucose oxidase-nafion composites, Applied Surface Science 470 (2019) 13–18.
[10] Alexander A Balandin, Phononics of graphene and related materials, ACS nano 14 (5) (2020) 5170–5178.
[11] N. Burger, A. Laachachi, M. Ferriol, M. Lutz, V. Toniazzo, D. Ruch, Review of thermal conductivity in composites: mechanisms, parameters and theory, Progress in Polymer Science 61 (2016) 1–28.
[12] A. Mora, F. Han, G. Lubineau, Computational modeling of electrically conductive networks formed by graphene nanoplatelet–carbon nanotube hybrid particles, Modelling and Simulation in Materials Science and Engineering vol. 26 (3) (2018), 035010.
[13] A. Mora, F. Han, G. Lubineau, Estimating and understanding the efficiency of nanoparticles in enhancing the conductivity of carbon nanotube/polymer composites, Results in Physics 10 (2018) 81–90.
[14] Vinod KS Shante, Scott Kirkpatrick, An introduction to percolation theory, Advances in Physics 20 (85) (1971) 325–357.
[15] Muhammad Sahimi, Heterogeneous Materials I: Linear Transport and Optical Properties, vol. 22, Springer Science & Business Media, 2003.
[16] Amnon Aharony, Dietrich Stauffer, Introduction to Percolation Theory, Taylor & Francis, 2003.
[17] A.G. Hunt, Continuum percolation theory for water retention and hydraulic conductivity of fractal soils: Estimation of the critical volume fraction for percolation, Advances in Water Resources 27 (2) (2004) 175–183.

[18] Hugo Fricke, A mathematical treatment of the electric conductivity and capacity of disperse systems i. the electric conductivity of a suspension of homogeneous spheroids,Physical Review 24(5) (1924) 575.
[19] A.G. Hunt, Continuum percolation theory for transport properties in porous media, Philosophical Magazine 85(29) (2005) 3409–3434.
[20] Michael A. Dubson, James C. Garland, Measurement of the conductivity exponent in two-dimensional percolating networks: square lattice versus random-void continuum, Physical Review B 32(11) (1985) 7621.
[21] Stephan Mertens, Cristopher Moore, Continuum percolation thresholds in two dimensions, Physical Review E 86 (6) (2012), 061109.
[22] A. Celzard, J.F. Marêché, Non-universal conductivity critical exponents in anisotropic percolating media: a new interpretation, Physica A: Statistical Mechanics and its Applications 317 (3–4) (2003) 305–312.
[23] M. Foygel, R.D. Morris, D. Anez, S. French, V.L. Sobolev, Theoretical and computational studies of carbon nanotube composites and suspensions: Electrical and thermal conductivity, Physical Review B 71 (10) (2005), 104201.
[24] L. Berlyand, K. Golden, Exact result for the effective conductivity of a continuum percolation model, Physical Review B 50 (4) (1994) 2114.
[25] A.J. Marsden, D.G. Papageorgiou, C. Vallés, A. Liscio, V. Palermo, M.A. Bissett, R. J. Young, I.A. Kinloch, Electrical percolation in graphene–polymer composites, 2D Materials 5 (3) (2018), 032003.
[26] D.S. McLachlan, Equations for the conductivity of macroscopic mixtures, Journal of Physics C: Solid State Physics 19 (9) (1986) 1339.
[27] D.S. McLachlan, Measurement and analysis of a model dual-conductivity medium using a generalised effective-medium theory, Journal of Physics C: Solid State Physics 21 (8) (1988) 1521.
[28] D.S. McLachlan, Equation for the conductivity of metal-insulator mixtures, Journal of Physics C: Solid State Physics 18 (9) (1985) 1891.
[29] Robert E. Meredith, Charles W. Tobias, Conductivities in emulsions, Journal of the Electrochemical Society 108(3) (1961) 286.
[30] Xu. Wenxiang, Zhigang Zhu, Dongyang Zhang, Continuum percolation-based tortuosity and thermal conductivity of soft superball systems: shape dependence from octahedra via spheres to cubes, Soft Matter 14 (43) (2018) 8684–8691.
[31] Ying Chen, Christopher A. Schuh, Diffusion on grain boundary networks: Percolation theory and effective medium approximations, Acta Materialia 54 (18) (2006) 4709–4720.
[32] Asimina Manta, Matthieu Gresil, Constantinos Soutis, Predictive model of graphene based polymer nanocomposites: electrical performance, Applied Composite Materials 24 (2) (2017) 281–300.
[33] Amirhossein Biabangard Oskouyi, Uttandaraman Sundararaj, Pierre Mertiny, Tunneling conductivity and piezoresistivity of composites containing randomly dispersed conductive nano-platelets, Materials 7 (4) (2014) 2501–2521.
[34] Jan Tobochnik, David Laing, Gary Wilson, Random-walk calculation of conductivity in continuum percolation, Physical Review A 41 (6) (1990) 3052.
[35] Rongwei Zhang, Wei Lin, Kyoung-sik Moon, C.P. Wong, Fast preparation of printable highly conductive polymer nanocomposites by thermal decomposition of silver carboxylate and sintering of silver nanoparticles, ACS Applied Materials & Interfaces 2 (9) (2010) 2637–2645.
[36] Ya-Fei Zhang, Yun-Hong Zhao, Shu-Lin Bai, Xiaowen Yuan, Numerical simulation of thermal conductivity of graphene filled polymer composites, Composites Part B: Engineering 106 (2016) 324–331.
[37] Wenkai Xiao, Xian Zhai, Pengfei Ma, Taotao Fan, Xiaotuo Li, Numerical study on the thermal behavior of graphene nanoplatelets/epoxy composites, Results in Physics 9 (2018) 673–679.
[38] Niwei Zhan, Bo Chen, Changzheng Li, Pei Kang Shen, Molecular dynamics simulations of the thermal conductivity of graphene for application in wearable devices, Nanotechnology 30(2) (2018) 025705.
[39] Te-Hua Fang, Zhe-Wei Lee, Win-Jin Chang, Chao-Chun Huang, Determining porosity effect on the thermal conductivity of single-layer graphene using a molecular dynamics simulation, Physica E: Low-dimensional Systems and Nanostructures 106 (2019) 90–94.
[40] Farrokh Yousefi, Farhad Khoeini, Ali Rajabpour, Thermal conductivity and thermal rectification of nanoporous graphene: A molecular dynamics simulation, International Journal of Heat and Mass Transfer 146 (2020), 118884.
[41] Asghar Aryanfar, I.I.I. William Goddard, Jaime Marian, Constriction percolation model for coupled diffusion-reaction corrosion of zirconium in pwr, Corrosion Science 158 (2019), 108058.
[42] Edsger W Dijkstra, et al., A note on two problems in connexion with graphs, Numerische mathematik 1 (1) (1959) 269–271.
[43] Zichao Pan, Dalei Wang, Rujin Ma, Airong Chen, A study on itz percolation threshold in mortar with ellipsoidal aggregate particles, Computers and Concrete 22 (6) (2018) 551–561.
[44] Artyom Plyushch, Patrizia Lamberti, Giovanni Spinelli, Jan Macutkevič, Polina Kuzhir, Numerical simulation of the percolation threshold in non-overlapping ellipsoid composites: toward bottom-up approach for carbon based electromagnetic components realization, Applied Sciences 8 (6) (2018) 882.
[45] Guo Qing, Zhang Zheng, Xu. Yue, Path-planning of automated guided vehicle based on improved dijkstra algorithm, in: 2017 29th Chinese Control and Decision Conference (CCDC), IEEE, 2017, pp. 7138–7143.
[46] Hwan Il Kang, Byunghee Lee, Kabil Kim, Path planning algorithm using the particle swarm optimization and the improved dijkstra algorithm, in: 2008 IEEE Pacific-Asia Workshop on Computational Intelligence and Industrial Application, vol. 2, IEEE, 2008, pp. 1002–1004.
[47] Huijuan Wang, Yu Yuan, Quanbo Yuan, Application of dijkstra algorithm in robot path-planning, in: 2011 Second International Conference on Mechanic Automation and Control Engineering, IEEE, 2011, pp. 1067–1069.
[48] Andrzej Katunin, Generalized chemical distance distribution in all-sided critical percolation clusters, in: AIP Conference Proceedings, vol. 1790, AIP Publishing LLC, 2016, p. 150002.
[49] Yulin Chen, Jyh-Yuan Chen, Towards improved automatic chemical kinetic model reduction regarding ignition delays and flame speeds, Combustion and Flame 190 (2018) 293–301.
[50] Lei Chen, Tao Liu, Xian Zhao, Inferring anatomical therapeutic chemical (atc) class of drugs using shortest path and random walk with restart algorithms, Biochimica et Biophysica Acta (BBA)-Molecular Basis of Disease 1864 (6) (2018) 2228–2240.
[51] Y.-B. Yi, A.M. Sastry, Analytical approximation of the two-dimensional percolation threshold for fields of overlapping ellipses, Physical Review E 66 (6) (2002), 066130.
[52] Lihua Shen, Zhangxin Chen, Critical review of the impact of tortuosity on diffusion, Chemical Engineering Science 62 (14) (2007) 3748–3755.
[53] L. De Backer, G. Baron, Effective diffusivity and tortuosity in a porous glass immobilization matrix, Applied Microbiology and Biotechnology 39 (3) (1993) 281–284.
[54] Hongyu Chen, Valeriy V. Ginzburg, Jian Yang, Yunfeng Yang, Wei Liu, Yan Huang, Libo Du, Bin Chen, Thermal conductivity of polymer-based composites: Fundamentals and applications, Progress in Polymer Science 59 (2016) 41–85.
[55] Kelsey Meeks, Michelle L. Pantoya, Micah Green, Jordan Berg, Extending the excluded volume for percolation threshold estimates in polydisperse systems: The binary disk system, Applied Mathematical Modelling 46 (2017) 116–125.
[56] Asghar Aryanfar, Sajed Medlej, Ali Tarhini, Ali Tehrani, Elliptic percolation model for predicting the electrical conductivity of graphene-polymer composites, Soft Matter (2021).
[57] Yu. Chen, Chen Dian-ren, Li Yang, Chen Lei, Otsu's thresholding method based on gray level-gradient two-dimensional histogram, in: Proceedings of the 2nd International Asia Conference on Informatics in Control, Automation and Robotics – Volume 3, CAR'10, IEEE Press, 2010, pp. 282–285.
[58] Y.-B. Yi, A.M. Sastry, Analytical approximation of the percolation threshold for overlapping ellipsoids of revolution, Proceedings of the Royal Society of London. Series A: Mathematical, Physical and Engineering Sciences 460(2048) (2004) 2353–2380.
[59] Milan Ambrožič, The percolation threshold in systems of permeable ellipses, The European Physical Journal Applied Physics 41 (2) (2008) 121–127.
[60] Evgeny Pervago, Aleksandr Mousatov, Elena Kazatchenko, Mikhail Markov, Computation of continuum percolation threshold for pore systems composed of vugs and fractures, Computers & geosciences 116 (2018) 53–63.
[61] Jianjun Lin, Huisu Chen, Measurement of continuum percolation properties of two-dimensional particulate systems comprising congruent and binary superellipses, Powder Technology 347 (2019) 17–26.
[62] W. Xia, M.F. Thorpe, Percolation properties of random ellipses, Physical Review A 38 (5) (1988) 2650.
[63] Jiantong Li, Mikael Östling, Precise percolation thresholds of two-dimensional random systems comprising overlapping ellipses, Physica A: Statistical Mechanics and its Applications 462 (2016) 940–950.
[64] Huan Pang, Tao Chen, Gangming Zhang, Baoqing Zeng, Zhong-Ming Li, An electrically conducting polymer/graphene composite with a very low percolation threshold, Materials Letters 64 (20) (2010) 2226–2229.
[65] Liberata Guadagno, Marialuigia Raimondo, Luigi Vertuccio, Marco Mauro, Gaetano Guerra, Khalid Lafdi, Biagio De Vivo, Patrizia Lamberti, Giovanni Spinelli, Vincenzo Tucci, Optimization of graphene-based materials outperforming host epoxy matrices, RSC Advances 5 (46) (2015) 36969–36978.
[66] Jie Wang, Chao Li, Jackie Li, George J Weng, Yu Su, A multiscale study of the filler-size and temperature dependence of the thermal conductivity of graphene-polymer nanocomposites, Carbon 2021.
[67] Junjie Chen, Xuhui Gao, Wenya Song, Effect of various carbon nanofillers and different filler aspect ratios on the thermal conductivity of epoxy matrix nanocomposites, Results in Physics 15 (2019), 102771.
[68] Hasan Babaei, Pawel Keblinski, J.M. Khodadadi, Improvement in thermal conductivity of paraffin by adding high aspect-ratio carbon-based nano-fillers, Physics Letters A 377 (19–20) (2013) 1358–1361.